AIAA-2005-1248
43rd AIAA Aerospace Sciences Meeting & Exhibit
January 10-13, 2005
Reno, NV

Numerical simulations of ice droplet trajectories and collection efficiency on aero-engine rotating machinery

A. Hamed*, K. Das, D. Basu****
Department of Aerospace Engineering and Engineering Mechanics
University of Cincinnati
Cincinnati, OH 45221-0070

ABSTRACT

This paper presents a methodology for three-dimensional numerical simulations of super-cooled water droplet trajectories through aeroengine rotating machinery. Both flow and droplets' governing equations are formulated and solved in the reference frame of rotating blades. A Eulerian-Lagrangian approach is used for the continuous and discrete phases with one-way interaction model to simulate the aerodynamic effects on the three-dimensional particle trajectories. A flux-based collection efficiency model is proposed for internal flows to enable the calculation of the amount of water that impinges the rotating and stationary blade surfaces. The methodology is applied to a transonic fan rotor and the computational results for the 3D flow field is compared with available experimental data. The computed droplet trajectories, rotor blade impingement locations, and the corresponding water collection efficiency are presented and compared for different droplet sizes.

INTRODUCTION

Concerns over ice accretion on aircrafts in inclement weather have spurred global interest in its numerical simulations[1-5]. Most investigations involve aero thermodynamic analysis of the flow around the body, prediction of droplet impingement rate on its surface, thermodynamic analysis of the water that freezes to ice. Computed parameters include droplet collection rate, droplet impingement limits and rime ice shape[6-11]. Kind et al.[12] gave a literature review of computational techniques in icing simulations. In general, the flowfield and the droplet trajectories are solved separately and the Lagrangian approach is used in the droplet trajectory simulations. The interaction between phases is modeled through mass, momentum and energy exchange. Da Silveria et al.[13] compared the predictions of various methods with available experimental data over a wing and a fuselage.

Ice accretion in aircraft engines raises additional safety and performance concerns. Fan and spinner ice shedding can cause mechanical damage. On the other hand, ice accretion on turbofan splitters and fan and booster vanes can result in slow acceleration and lead to compressor stall. The simulation of ice accretion in aircraft engines is challenging because of the complex 3D unsteady turbomachinery flow and the effects of rotation on droplet trajectories.

Solid particles dynamics in aeroengine turbomachinery have been studied to investigate the associated blade surface erosion[14,15]. Unlike supercooled droplets, solid particles rebound after impacting the blade surfaces and continue their trajectories through succeeding blade rows[16,17]. Several factors affect the pattern and intensity of blade erosion including particle size blade material and blade row location[14,15,18]. Erosion damage in fan and compressor blades is manifested in pitting of leading edges and blade chord reduction. Numerical models have been developed for simulating the associated loss in aerodynamic performance[19].

**AIAA Fellow, Professor*
***AIAA Student Member, Graduate Student*

This paper presents a computational method for 3-D droplet trajectories through turbo-machines and the associated blade surface collection efficiency. Both flow and droplets' governing equations are formulated and solved in the reference frame of the rotating blades. A Eulerian-Lagrangian approach is used for the continuous and discrete phases with one-way interaction model to simulate the aerodynamic effects on the three-dimensional droplet trajectories. Computational results for the flow field and droplet trajectories relative to the rotor blades are presented for a modern turbofan rotor. A flux-based collection efficiency model is proposed to enable the calculation of the amount of water that impinges the blade surface.

METHODOLOGY

Both flow and particle governing equations are formulated in the rotating blade frame of reference. A Eulerian-Lagrangian approach is employed for the flow field and droplet trajectories. A one-way interaction model simulates the effects of aerodynamic forces on the droplet trajectories The compressible turbulent 3-D flow field through the rotor blade passage is obtained from the numerical solution of the Reynolds Averaged Navier Stokes (RANS) equations with periodic boundary conditions and radial equilibrium for the static pressure at the exit station. A flux based collection efficiency model is proposed to enable the calculation of water accumulation over the blade surface from the impingement statistics of sufficient number of droplets trajectories.

Turbomachinery Flow

The flow through a modern aeroengine fans is unsteady, three-dimensional with shock waves across the passages. A number of steady three-dimensional viscous flow analysis were reported for transonic fan flow[20,21,22]. The Runge-Kutta scheme has been used in many studies because of CPU economy and the ease of implementing convergence acceleration techniques.

In the current investigation, the aerodynamic solution of the turbomachinery flow field is obtained from the 3-D solution of the compressible Reynolds Averaged Navier Stokes (RANS) equations using ADPAC[23]. The code utilizes finite volume, Runge-Kutta time marching scheme to solve the time dependent form of 3-D RANS equations. Convective fluxes are approximated using a second order central difference scheme stabilized with scalar artificial dissipation. Local time stepping, implicit residual smoothing, scaled dissipation function, and a multigrid technique are employed to accelerate convergence. The algebraic Baldwin-Lomax model, one equation Spalart-Allmaras model and two-equation k-R model are available in the solver. Previous simulations by Yeuan et al.[24] of rotor 67 flow field using both low Reynolds number k-ε and Baldwin-Lomax turbulence models have indicated that the predicted aerodynamic performance as well as the 3-D shock structure within the rotor passage were comparable for both turbulence models over a wide range of operating conditions. On the other hand, Hamed and Vogiatzis[25] concluded that the two-equation turbulence model gave better agreement with the experimentally measured surface pressure distribution in the case of shock-induced massive flow separation over 2D-CD nozzle flaps. Since such conditions are generally not encountered in high performance turbomachinery the Baldwin – Lomax turbulence model was used in the present investigation. It was concluded that the Baldwin-Lomax algebraic turbulence model enables a considerable reduction in the required computational resources without sacrificing the fidelity of the 3-D flow solution.

Droplet Trajectories

The droplet trajectories are determined from the numerical integration of the equations of motion in the blade rotating reference frame[14]:

$$\frac{d^2 r_p}{d\tau^2} = F_r + r_p\left(\frac{d\theta_p}{d\tau} + \omega\right)^2 \qquad (1)$$

$$r_p \frac{d^2\theta_p}{d\tau^2} = F_\theta - 2\frac{dr_p}{d\tau}\left(\frac{d\theta_p}{d\tau} + \omega\right) \qquad (2)$$

$$\frac{d^2 z_p}{d\tau^2} = F_z \qquad (3)$$

The same equations of motion can be applied to stationery turbomachinery blades by setting $\omega=0$ and replacing the velocity by the absolute gas velocity. In the above equations, r_p, θ_p and z_p define the particle location in cylindrical coordinates, and ω the blade angular velocity. The last term in the RHS of the first two equations represent the centrifugal force and Coriolis acceleration. The first term on the RHS

of equations 1-3 represents the components of the aerodynamic force of interaction between the two phases. The drag due to the relative velocity is considered as the primary aerodynamic force on the droplets since the forces due to gravity and buoyancy are negligible compared to the aerodynamic and centrifugal forces[14,15]. Forces due to inter-droplet interactions and pressure gradient are also negligible for the small supercooled water droplets. The aerodynamic force of interaction is expressed in terms of the drag coefficient and the droplet slip velocity as follows[15]:

$$\overline{F} = \frac{3}{4}\frac{C_D}{d}\left|\overline{V} - \overline{V}_p\right|.\left(\overline{V} - \overline{V}_P\right) \qquad (4)$$

Where d is the particle diameter and $\overline{V}$ and $\overline{V}_P$ are the gas and the droplet velocity vectors. The drag coefficient C_D is computed from empirical correlations involving the Reynolds number based on the relative velocity between the droplet and the gas.

The droplets equations of motions are solved using a four-stage Runge-Kutta time integration. At every time step the blade surfaces are scanned to determine their relative position to the droplet. Once the droplet reaches a solid surface, trajectory computations are terminated and the impact location is recorded. Similarly, if a droplet exits from the blade passage, the exit point is recorded. The outlined droplet trajectory simulation procedure was implemented in the code TURBODROP that was run in parallel on a Linux cluster using the Portland Fortran-90 compiler auto-parallelization.

Collection Efficiency

It has been a common practice in external flows[9,12] to initiate a number of droplet trajectories, which are released over incremental distance across the free stream direction, until the limiting droplet trajectories define those that reach the surface outermost boundaries. The slopes of the computed trajectories relative to the free stream direction are used to define collection efficiency for ice-growth calculations. The collection efficiency is typically less than one, which is the upper limit had the droplets not been deflected by the flow around the surface.

The concept of limiting droplet trajectories in the particle frame of reference is not applicable to the moving rotor blades. In addition, neighboring droplets could continue their trajectories in different blade passages of subsequent blade rows. Therefore the collection definition that has been used in external flows is not applicable to rotating machines. A mass flux based collection efficiency is better suited for internal flow applications and could be equally applicable to both rotating and stationary blades. A flux based collection efficiency model based on the ratio of the local droplet mass flux at the blade surface to its value at the inlet station was used to compute the water mass accumulation rate on the rotor blade surface.

Numerics

The outlined methodology was used in the numerical simulations for NASA rotor-67. Detailed experimental LDV measurements through the rotor passages were reported for this rotor by Straziser et al.[26]. The total temperature and the total pressure profiles were specified at the inlet based on the experimental data. Adiabatic wall boundary conditions were used, with no-slip at the stationary walls, and prescribed rotational speed at the rotating wall. The exit static pressure was specified at the tip, and the redial pressure distribution was determined from the integration of the axisymmetric radial momentum equation. Periodic boundary conditions were employed in the blade-to-blade directions.

The solution domain for the both 3D flow and droplet trajectory simulations extended 80% chord upstream and 45% chord downstream of the rotor blade row. Figure 1 shows the computational grid consisting of 145 × 65 × 65 grid points in the stream-wise, blade-to-blade and the hub-to-tip directions. The grid was stretched in the near wall regions using a hyperbolic tangent function. The minimum grid spacing in the wall normal direction was 1.0×10^{-4} times the chord with 15 grid points within the boundary layer.

RESULTS AND DISCUSSIONS

Rotor-67 is the first stage rotor of a two-stage fan, with a design pressure ratio of 1.63 and a mass flow rate of 33.25 kg/sec[26]. The tip radius varies from 25.7 cm at the leading edge to 24.25 cm at the trailing edge, and the hub/tip ratio varies from 0.375 to 0.478. It has 22 blades with

1.56 aspect ratio. Its design 16043 RPM corresponds to a rotor tip speed of 429 m/sec and a relative inflow Mach number of 1.38 at the tip.

Figure 2 shows the meridional view of test fan rotor with the aerodynamic survey locations. The computed static pressure ratio behind the rotor blade is shown in figure 3. One can see that the computed profile is in close agreement with the experimental results.

Figure 4 presents the computed and experimentally measured flow relative Mach number contours at 30% and 70% span from the tip. One can observe a significant span-wise variation in the rotor flow field. The relative inlet Mach number is 1.2 at 30% span and 0.95 at 70% span. A complex shock structure can be seen at 30% span with a bow wave ahead of the blade and a normal shock inside the blade passage. A small bubble forms on the forward portion of the suction surface at 70% span, and the flow separates from the blade suction surface.

Sample computational results are presented for 15μm and 50μm droplet trajectories through the rotor. The droplets were injected with zero velocity at the computational upstream boundary and were uniformly distributed laterally for uniform influx. Figures 5 and 6 show sample droplet trajectory projections at 30% and 70% blade span. One can see that the droplets enter the blade passage with a positive incidence angle in the rotor reference frame. This is a result of their lower absolute velocities compared to the flow. The velocity lag is greater for the larger particles and consequently more (97.25%) of the 50 micron droplets impinge the rotor blade compared to 64.35% of the 15 micron droplets.

Figures 7 and 8 show the impingement locations for 15 and 50-micron droplets. In general most impingements occur on the rotor blade pressure surface, with very few near the leading edge of the suction surface. One can see that the 15-micron particles impinge most of the blade pressure surface except for a small region towards the trailing edge near the hub. The extent of the pressure surface impingement region is smaller for the 50-micron droplets.

The computed flux based collection efficiency is shown in Figures 9 and 10 for 15 and 50-micron droplets respectively. The collection efficiency contours cover more of the blade suction surface for the 15μm droplets but their mean value is lower in comparison to the 50-micron case.

CONCLUSIONS

A numerical methodology is presented for the simulations of supercooled droplet trajectories through aero engine rotating machinery. A flux-based definition of collection efficiency is proposed for the rotating blades. Computational results are presented for NASA transonic rotor-67 at peak efficiency. The relative Mach number contours and the static pressure ratio profile show large radial variations in the flow field and 3-D shock structure in the fan rotor.

Droplet trajectories, rotor blade surface impingement statistics, and collection efficiency are computed for two droplet mean diameters. The results show that more of the larger droplets impinge on the rotating blade surface. Consequently water accumulation is higher for the larger droplets. On the other hand, the collection efficiency is lower for the smaller particles, but they impinge more of the blade pressure surface.

ACKNOWLEDGEMENTS

This research was sponsored by Ohio Aerospace Institute grant CCRP 2003-05. The authors would like to thank Dr. Kattalaicheri Venkataramani of GE Aircraft Engines, Cincinnati for many useful discussions and Mr. Robert Ogden of UC for his technical support.

REFERENCES

1) Gent, R.W. “TRAJICE2-A combined water droplet and ice accretion prediction code for airfoils”, Royal Aerospace Establishment TR 90054, 1990.
2) Brahimi, N.T., Tran, P., and Paraschivoiu, I., “Numerical Simulation and Thermodynamic Analysis of Ice Accretion on Aircraft Wings”, Center de Development Technologique de Ecole Polytechnique de Montreal, Final report C.D.T Project C159, 1994.
3) Bourgault, Y., Habashi W.G., Dompierre J., Boutanios Z, Di Bartolomeo W., “An Eulerian Approach to Supercooled Droplets Impingement Calculations”, AIAA Paper-97-0176, 1997.

4) Caruso, S.C. “NEARICE-An Unstructured Mesh Navier-Stokes Based Ice Accretion Prediction Method”, AIAA Paper no 94-0606, 1994.
5) Guffond D., et Bruent L., “Validation du Programme Bidimensional de Captition”, ONERA RT no. 20/5146 SY, 1985.
6) Ruff, G.A., and Berkowitz, B.M., “User’s Manual for the NASA Lewis Ice Accretion Prediction Code (LEWICE)”, NASA-CR-185129, May 1990.
7) Potapczuk, M.G., and Bidwell, C.S, “Numerical Simulation of Ice Growth on a MS-317 Swept wing Geometry” NASA-TM-103705, 1991.
8) Chung, J. and Addy, Jr, H.E. “A Numerical Simulation of Icing Effects on a Natural Laminar Flow Airfoil”, 2000, NASA TM-2000-209775.
9) Bidwell C.S and Mohler S.R. ‘Collection Efficiency and Ice Accretion Calculations for a Sphere, a Swept MS(1)-317 Wind, a Swept NACA 0012 Wing Tip, an Axisymmetric Inlet and a Boeing 737-200 Inlet” NASA TM-106821, 1995.
10) Flemming, R.J., and Lednicer, D.A., “High Speed Ice Accretion on Rotorcraft Airfoils,” NASA CR-3910, Aug. 1985.
11) Flemming, R. J.; Shaw, R. J.; Lee, J. D., “The performance characteristics of simulated ice on rotorcraft airfoils”, NASA CR-0101, Aug. 1985.
12) Kind, R.J., Potapczuk, M.G., Feo, A, Golia, C. and Shah, A.D. “Experimental and Computational Simulation of in-flight Icing Phenomena”, Progress in Aerospace Sciences vol. 34. 1998. pp 257-345.
13) Da Silveira, R.A., Maliska, C.R., Estivam, D.A., Mendes, R., “Evaluation of Collection Efficiency Methods for Icing Analysis”, Proceedings of 17th International Congress of Mechanical Engineering, November 10-14, 2003, Sao Paulo.
14) Hamed, A. and Tabakoff, W., “Experimental and Numerical Simulations of the Effects of Ingested articles in Gas Turbine Engines,” AGARD CP 558, “Erosion, Corrosion and Foreign Object Damage in Gas Turbines,” November, 1994.
15) Tabakoff, W., Hamed, A., & Wenglarz, R., "Particulate Flows, Turbomachinery Erosion and Performance Deterioration," Von Karman Lecture Series 1988-89, May 24-27, 1988, Brussels, Belgium.
16) Tabakoff, W., Hamed, A. & Metwally, M., "Effect of Particle Size Distribution on Particle Dynamics and Blade Erosion in Axial Flow Turbines," Journal of Gas Turbine and Power, Vol. 113, October 1991, pp. 607-615.
17) Hamed, A. & Kuhn, T.P., “Effects of Variational Particle Restitution Characteristics on Turbomachinery Erosion,” Journal of Engineering for Gas Turbines and Power, July 1995, Vol. 117, pp. 432-440.
18) Hamed, A., Jun, Y. D., and Yeuan, J, J., “Particle Dynamics Simulations in Inlet Separator with an Experimentally Based Bounce Model”, 1993, AIAA-1993-2156.
19) Hamed, A., Tabakoff, W., and Singh, D., “Modelling of Compressor Performance Deterioration Due to Erosion,” International Journal of Rotating Machinery, Vol. 4, November 1998, pp. 243-248.
20) Chima, R.V., “Viscous Three-Dimensional Calculations of Transonic Fan Performance,” 1992, in CFD Techniques for Propulsion Applications, AGARD Conference Proceedings No. CP-510, AGARD, Neuilly-Sur-Seine, France, pp. 21-1 to 21-19.
21) Jennions, I. K., and Turner, M. G., “Three-Dimensional Navier-Stokes Computations of Transonic Fan Flow Using an Explicit Flow Solver and an Implicit k-ε solver”, Journal of Turbomachinery, 1993, Vol. 115, pp. 261-272.
22) Arnone, A., “Viscous Analysis of Three-Dimensional Rotor Flows Using a Multigrid Method,” 1993, ASME Paper No. 93-GT-19.
23) Hall, E.J., Lynn, S.R., Heidegger, N.J. and Delaney, R.A., “ADPAC v1.0-User’s Manual”, NASA-CR-1999-206600.
24) Yeuan, J, J, Liang, T., and Hamed, A., “Viscous Simulations In a Transonic Fan Using k-ε and algebraic turbulence models”, 1998, AIAA-98-0932.
25) Hamed, A., and Vogiaztis, C., “Assessment of Turbulence Models in Overexpanded 2D-CD Nozzle flow Simulations”, 1995, AIAA-1995-2615.
26) Straziser, A. J., Wood, J. R., Hathaway, M. D., and Suder, K. L., “Laser Anemometer Measurements in a Transonic Axial Flow Fan Rotor,” 1989, NASA Technical paper 2879.

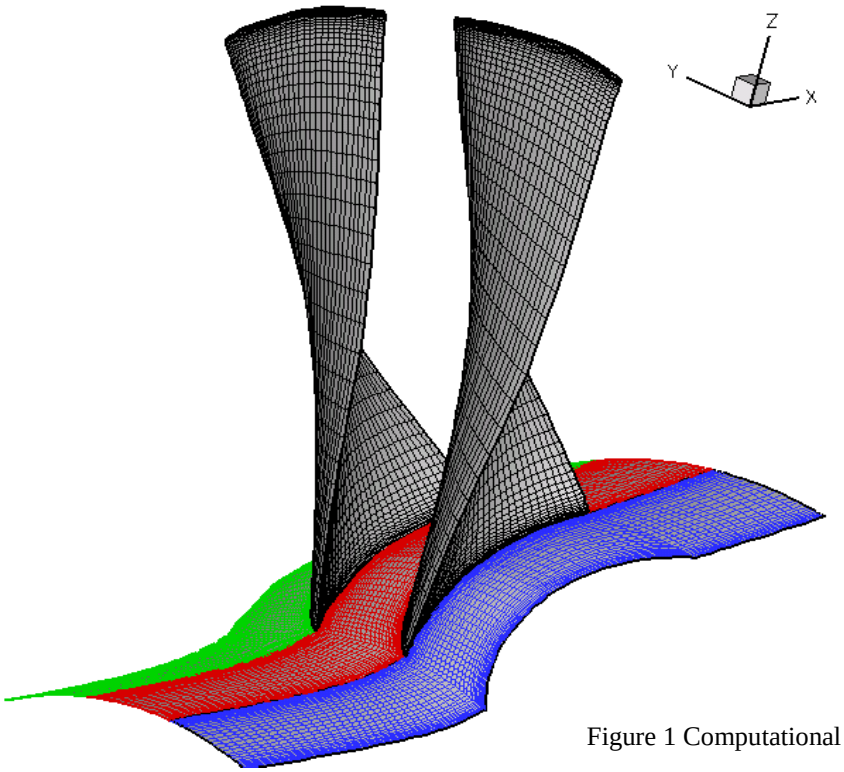

Figure 1 Computational Grid

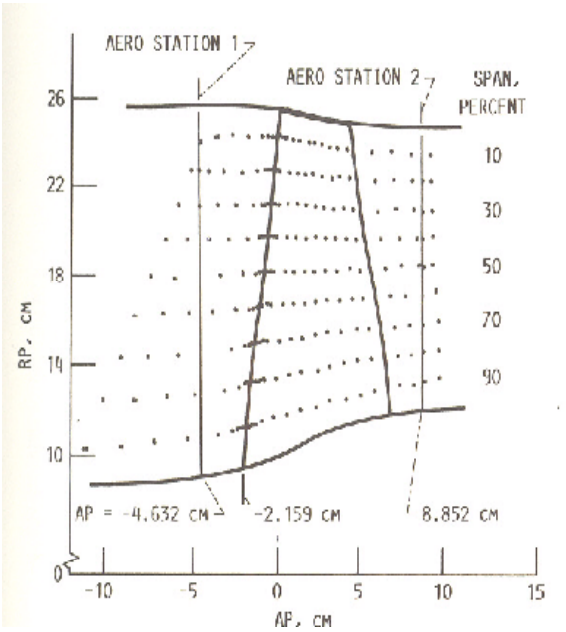

Figure 2 Meridional view of the test fan rotor showing laser anemometer and aerodynamic survey locations (26)

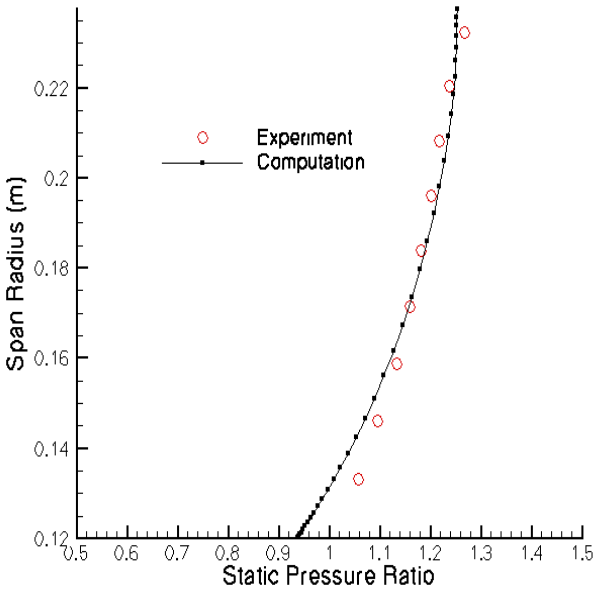

Figure 3 Static Pressure Profiles at Aero Station 2: Comparison with experimental data

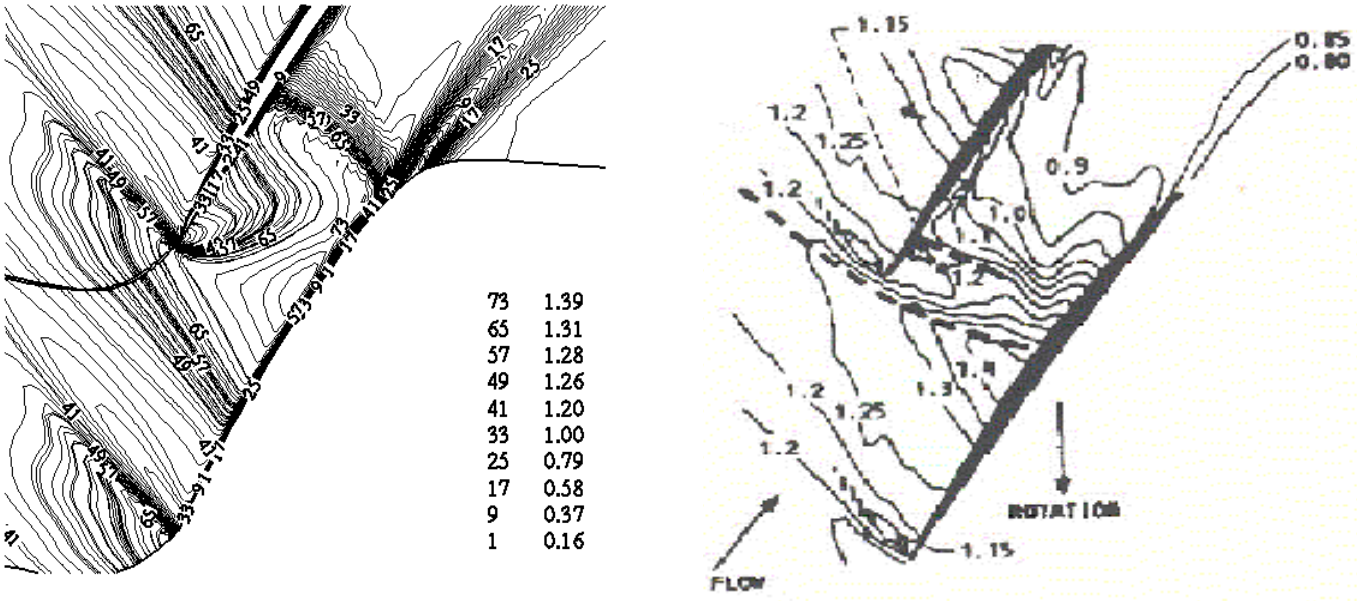

30% span from shroud

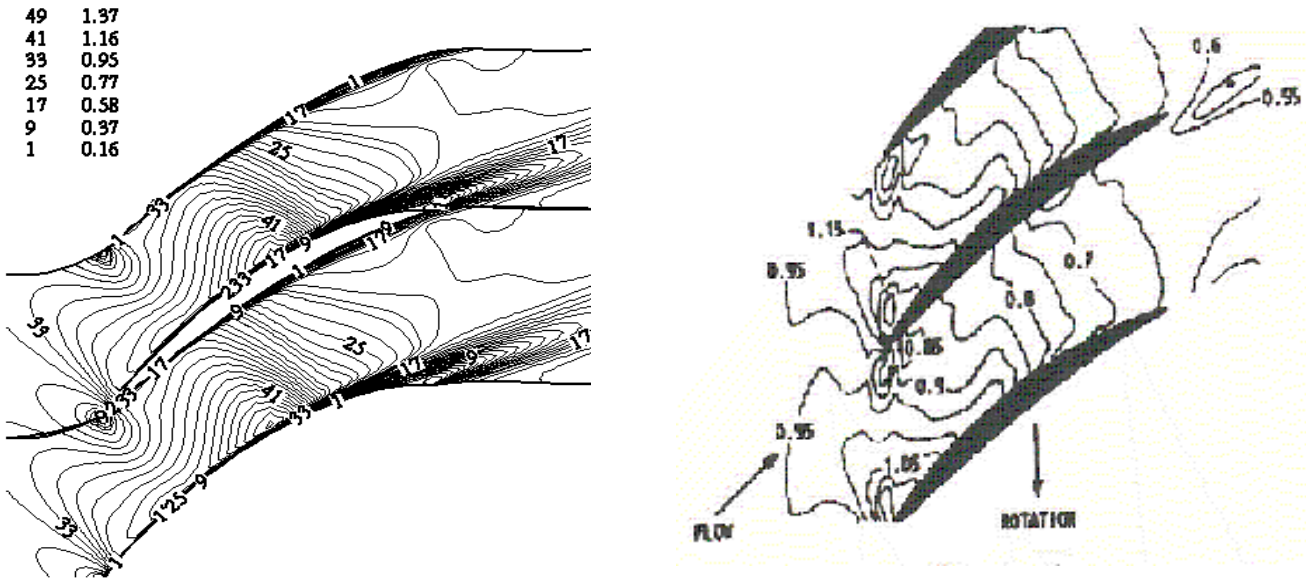

70% Span from shroud

Computation Experiment

Figure 4 Experimental and Computed Contours of Relative Mach number

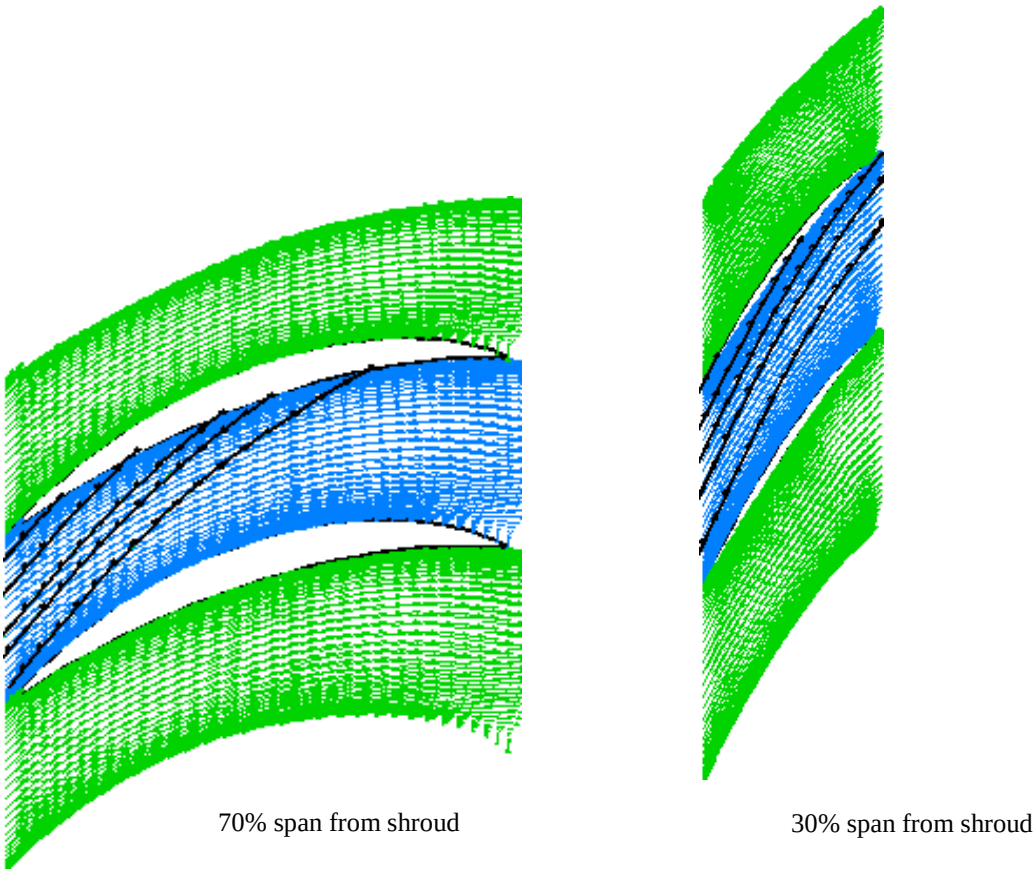

70% span from shroud 30% span from shroud

Figure 5 Sample droplet trajectory projections inside the blade for 15-micron

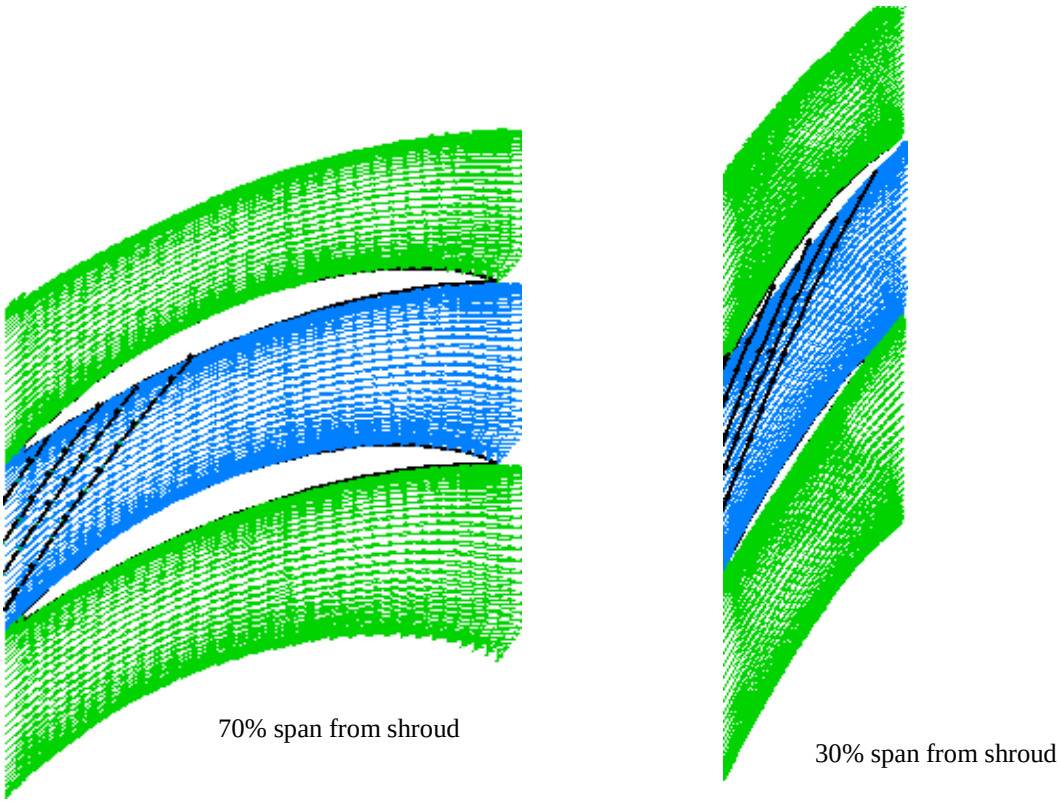

70% span from shroud 30% span from shroud

Figure 6 Sample droplet trajectory projections inside the blade for 50-micron

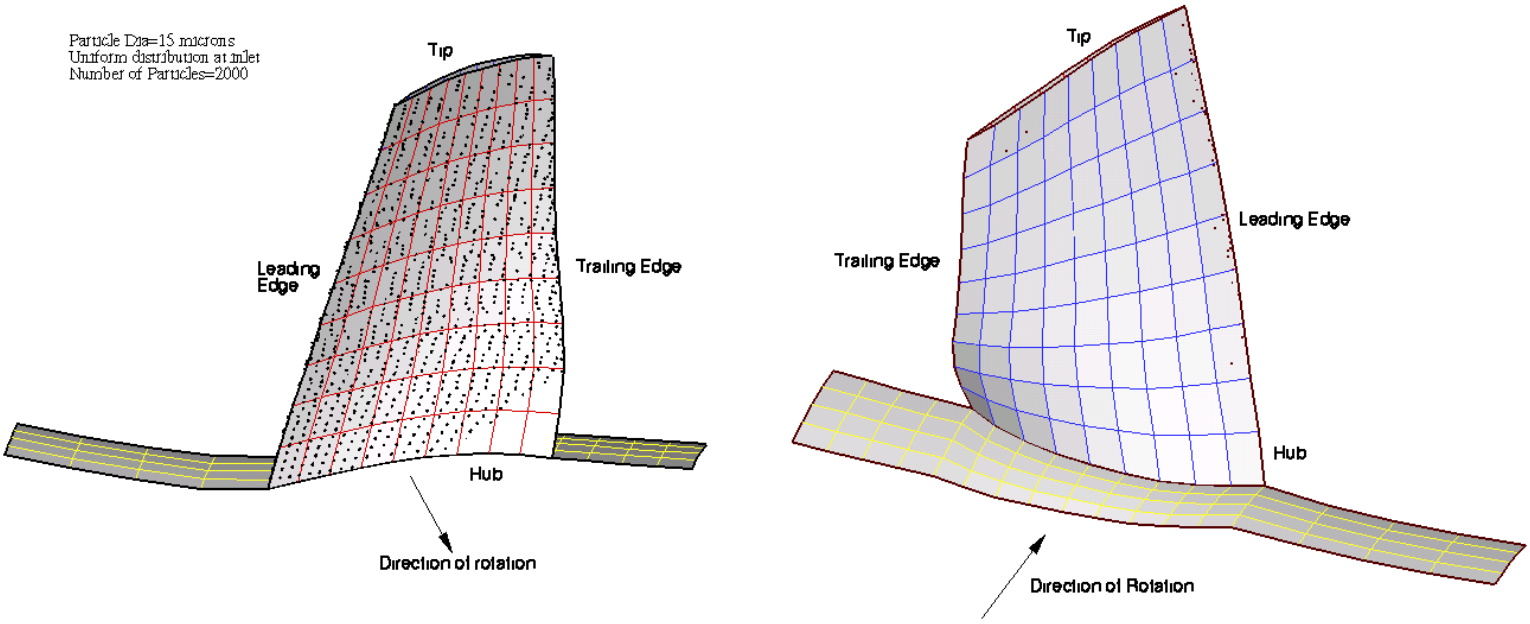

Pressure Surface

Suction Surface

Figure 7 Impingement Locations for 15 micron droplets

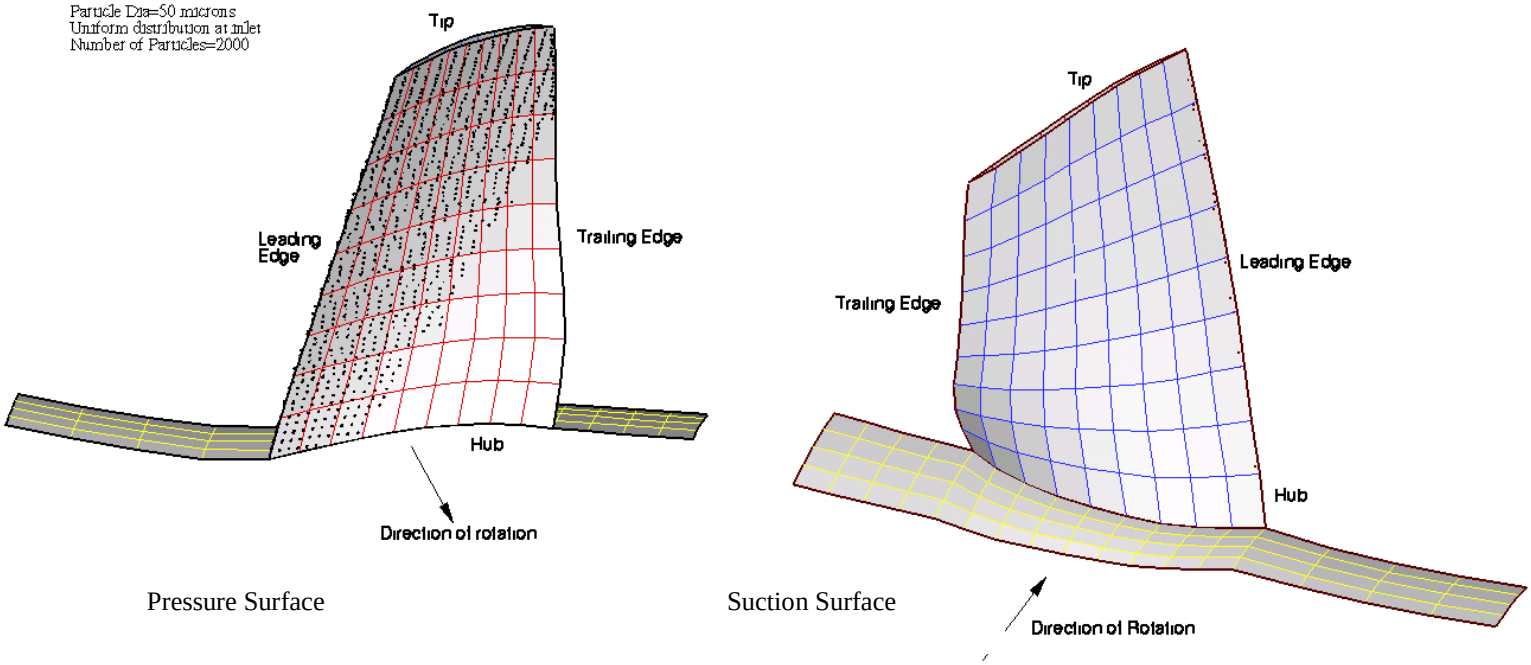

Pressure Surface

Suction Surface

Figure 8 Impingement Locations for 50 micron droplets

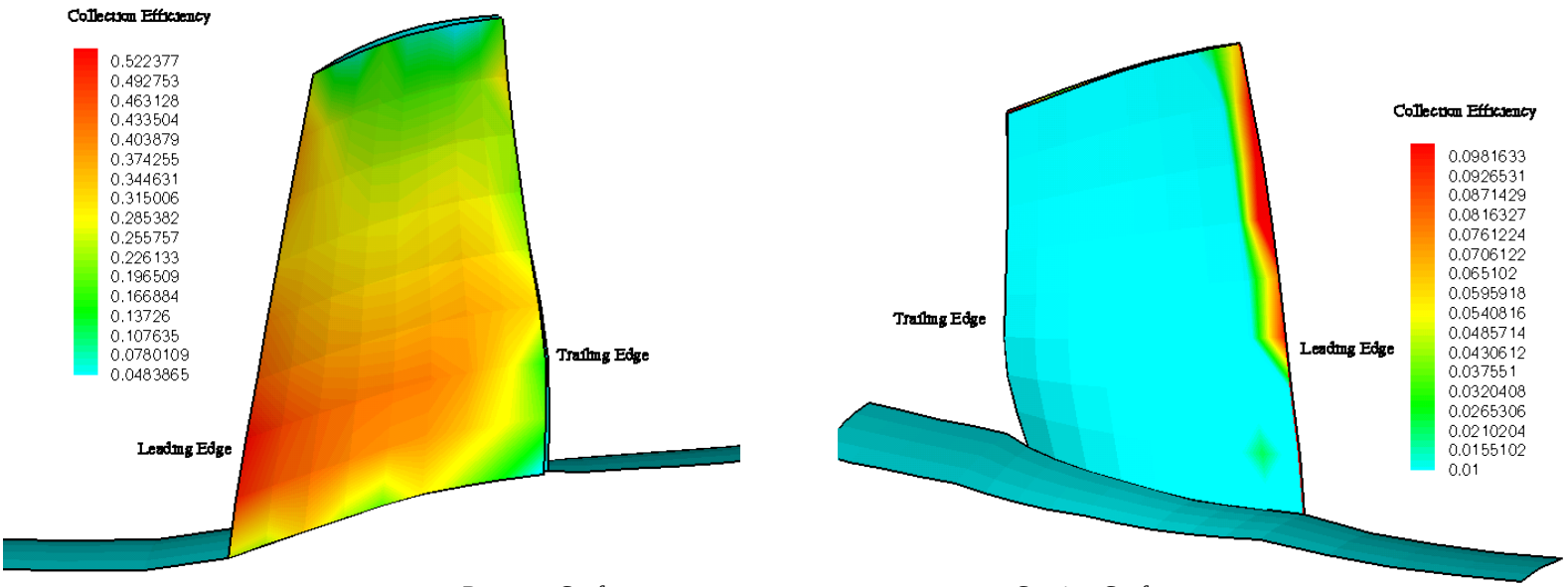

Pressure Surface Suction Surface

Figure 9 Blade Collection Efficiency for 15-micron droplets

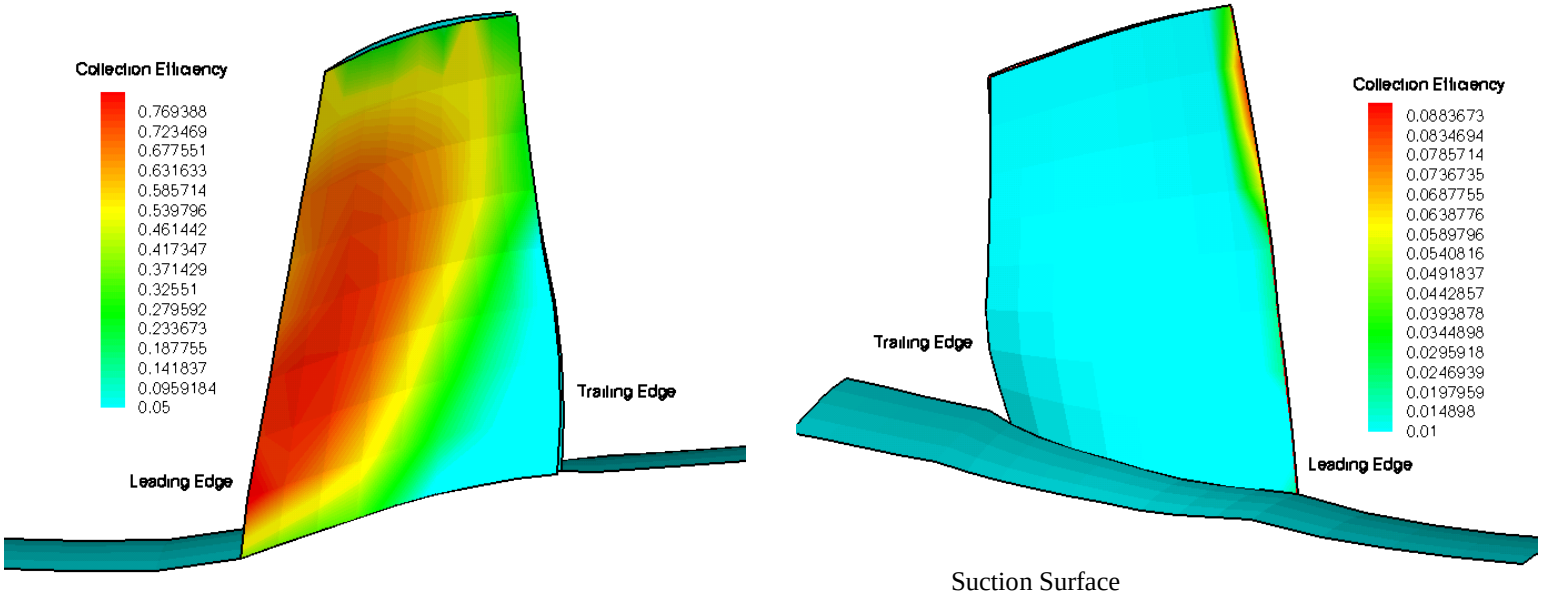

Pressure Surface

Suction Surface

Figure 10 Blade Collection Efficiency for 50-micron droplets